Integrating physical circulation models and genetic approaches to investigate population connectivity in deep-sea corals

Annalisa Bracco*[1], Guangpeng Liu[1], Matthew P. Galaska[2], Andrea M. Quattrini[3], Santiago Herrera[2]

1 School of Earth and Atmospheric Sciences, Georgia Institute of Technology, 311 Ferst Dr, Atlanta, GA 30332, USA

2 Department of Biological Sciences, Lehigh University, Bethlehem, PA 18015, USA

3 Department of Biology, Harvey Mudd College, 1250 N. Dartmouth Ave., Claremont, CA, USA

*abracco@gatech.edu

Abstract

Deepwater corals are found on hard grounds of the continental shelf and slope of all ocean basins, where they enhance the abundance and biodiversity of invertebrates and fishes. Despite their essential role in deep-sea ecosystems, the knowledge of the factors that promote or impede connectivity among discrete coral communities remains elusive. Logistical challenges prevent a direct quantification of the essential factors affecting connectivity, such as timing of spawning, time spent in the water column, and settlement behavior, as well as the details of the physical environment and its variability.

This study argues that an integrated framework including population genetic approaches and physical models of the ocean circulation with larval particle tracking capabilities can enhance our understanding. Genetic approaches allow determination of general time-integrated patterns of dispersal distance and direction in virtually any species, while transport models can refine understanding of the processes behind the observed dispersal patterns. Here, this integrated approach is applied towards investigating the connectivity of a deepwater coral, *Callogorgia delta,* along the upper continental slope of the northern Gulf of Mexico. The circulation in the basin is simulated by a regional ocean model at 1 km horizontal resolution, which is sufficiently detailed to allow for the generation and evolution of submesoscale eddies and vorticity filaments, and for a

reliable representation of major bathymetric features. Building upon data from four sites spanning about 250 km of distance and 400 m of depth, it is concluded that depth differences on scales of tens to at most few hundreds of meters are sufficient to limit *C. delta* connectivity among sites. This result has important implications in the development of restoration and preservation strategies of deepwater corals in the Gulf of Mexico and calls for carefully accounting for the depth dimension in these efforts.

1. Introduction

Coastal regions in the world have experienced environmental catastrophes in recent history, from prolonged periods of above-average water temperatures, to anoxic events, and man-made pollution episodes. The Gulf of Mexico (GoM) is no exception, having sustained, eutrophication and anoxic events, increased surface temperatures, and a number of oil spills, including the largest ever recorded, following the explosion of the Deepwater Horizon platform in 2010. With continued anthropogenic threats in the marine environment coupled with global ocean change, there is an urgent need to develop scientific frameworks that allow for informed decisions about the management and conservation of vulnerable marine ecosystems in the world, and in the GoM in particular.

Deepwater corals (i.e. heterotrophs living deeper than 50 m) are commonly found in discrete and spatially separated communities on hard grounds of the continental shelves and slopes around the globe. They play a foundational role in marine ecosystems by generating three-dimensional structures that provide habitats for diverse and abundant invertebrate and fish communities, including refuge and prey for commercially valuable fisheries (Baillon et al., 2012; Cordes et al., 2008; Krieger and Wing, 2002; Ross and Quattrini, 2009; Stone, 2006). Each community serves as a biodiversity hotspot by locally enhancing the abundance and diversity of invertebrates and fishes (Cordes et al., 2008; Demopoulos et al., 2014; Henry and Roberts, 2007; Rowden et al., 2010). Knowledge of the factors that promote or impede the connectivity of these discrete, deepwater benthic communities is essential to ensure the resilience and sustainability of marine ecosystems (Gaines et al., 2010; Kinlan et al., 2005). Connectivity among deepwater coral populations contributes to their ability to adapt to natural and anthropogenic stressors (Herrera & Shank, 2016; Morrison et al. 2011; Quattrini et al. 2015). Genetic structuring of corals by depth has received interest in recent years as part of the exploration of recovery strategies for shallow reefs subject to major perturbations (e.g. Costantini et al., 2016; Bongaerts et al. 2017, Yesson et al. 2018), under the hypothesis that deep coral reefs could act as refuges during disruptive events that impact shallower reefs. Determining the distance, rate and directionality of larval dispersal is therefore central to understanding how coral populations are interconnected and the degree of resiliency in the event of a perturbation, natural or anthropogenic.

68 Here, we argue that the most effective way to estimate the connectivity in deepwater
69 populations is through an integrated, multidisciplinary framework. This is because time of
70 spawning, time spent by larvae in the water column, and settlement behavior are difficult to
71 predict and logistically challenging to observe, particularly in the deep sea. Physical models of
72 ocean circulation coupled with tracking of virtual larval particles allows for exploring potential
73 population connectivity, while the use of population genetic approaches provide a measurement
74 of realized connectivity and can guide the modeling set-up and testing of predictions. The
75 population genetic approach allows determination of general time-integrated patterns of dispersal
76 in virtually any biological species, while the transport model, if sufficiently realistic and detailed,
77 allows refinement of our understanding of the processes – physical and biological - behind the
78 inferred connectivity patterns. This combined approach has been applied in recent years in
79 handful of studies of shallow-water species (White et al., 2010; Waters et al., 2014; Lal et al.,
80 2017; Jahnke et al., 2018; Sinclair et al., 2018), but is not yet common in the investigation of
81 connectivity in deeper waters (> 50 m) (but see Cardona et al. 2016). The reason behind is likely
82 two-fold: on one hand a smaller number of genetic studies are available for deepwater species
83 due to their costs and logistical challenges, on the other modeling investigations require high
84 resolution to capture the bathymetric details likely relevant to larval dispersal and are difficult to
85 validate due to the limited amount of quality-controlled in-situ data below the mixed-layer. In the
86 deep GoM, however, Cardona et al. (2016) showed that an integrated approach can help identify
87 potential physical or biological barriers to dispersal, while contributing information at spatial and
88 time scales relevant to resource managers and stakeholders.
89
90 In this study, we provide a novel application of such integrative framework focusing on the
91 population connectivity of a deepwater coral, *Callogorgia delta. C. delta* is one of the most
92 abundant corals occurring along the upper continental slope (400 – 900 m) of the northern GoM.
93 Quattrini et al. (2015) examined the patterns of population genetic structuring in this species by
94 recovering DNA microsatellite data from individuals collected from multiple sites in the GoM. This

study revealed a pattern of isolation by depth between coral aggregations found at lease blocks[1] GC235 (Green Canyon block 235, 532 m depth) and GC249 (Green Canyon block 249, 789 m depth), separated geographically by ~ 67 km, but also between aggregations at MC751 (Mississippi Canyon 751, 440 m depth) and MC885 (Mississippi Canyon 885, 629 m depth), which are only 15 km apart. This pattern, however, could not be unequivocally attributed to limited gene-flow caused by oceanographic processes and separation among sites or to adaptive divergence in the presence of gene flow, because microsatellite data cannot be used to determine selection (microsatellites are DNA sequence repeats) and an ocean circulation model was not included in the study. Here we revisit the patterns of realized connectivity of this species with new genome-wide restriction site associated DNA sequencing (RAD-seq) data collected in 2017. We integrate these results with a numerical model of the ocean circulation of the GoM coupled to a larval-transport tracking algorithm to investigate the mechanisms behind the observed patterns in gene flow.

In this work, the physical dispersal model simulates the circulation in the GoM basin at 1 km horizontal resolution, allowing for the generation and evolution of submesoscale eddies and vorticity filaments, and for a realistic representation of lateral and vertical transport barriers associated with bathymetric features (Bracco et al., 2016). In the GoM the basin-wide circulation in the upper 1000 m (the depth range of interest for this work) is dominated by the presence of the Loop Current (LC), that flows into the basin through the Yucatan Channel and exits it through the Florida Straits. The LC transports approximately 25 x 10^6 m^3s^{-1} of warm and salty water from the equatorial Atlantic (Johns et al., 2002) into the GoM. Instabilities and interactions of the LC with the bathymetry induce on average once every 10-11 months the detachment of large anticyclonic eddies with diameter of about 300 km (Cardona and Bracco, 2016; Donohue et al., 2016). These Loop Eddies or Rings can live for over a year, extend vertically to about 1000 m and move westward until they interact with the continental shelf and lose their coherency.

[1] Blocks are used by the Bureau of Ocean and Energy Management (BOEM) to define small geographic areas for leasing and administrative purpose. Coral sites are identified based on the blocks they belong to.

At scales of a few kilometers, and over the continental slope whenever the water column is less than ~ 1000 m in depth and therefore too shallow to allow for the penetration of the LC and Rings, submesoscale filaments and eddies are prevalent in the vorticity field (Bracco et al., 2016). Submesoscale circulations have scales of few hundred meters to few kilometers and a local Rossby number ($R_o=u/Lf$, where L is the scale of the circulation considered, f the Coriolis parameter and u the lateral flow velocity) of order O(1). They emerge at the ocean vertical boundaries whenever density gradients are present from a range of instability mechanisms (see Bracco et al., 2019 for a review focused on the GoM).

Submesoscale circulations near the ocean surface extend vertically into the mixed layer, and only when associated to the LC and Rings may approach the depths of the coral colonies. They are key contributors, however, to vertical transport in the upper ~ 500 m (Zhong and Bracco, 2013; Liu et al., 2018; Bracco et al., 2019). At the depths of interest, currents are mostly along-shore and not generally coherent with the surface ones (e.g. Cardona and Bracco, 2016). Cross-shore currents are weak and, when present, are associated with mesoscale eddies impinging or forming on the shelf (Ohlmann et al., 2001; Hamilton et al., 2002; Bracco et al., 2016), as confirmed by drifter deployments (DeHaan and Sturges, 2005, Ohlmann and Niiler, 2005). Near-bottom submesoscale features form in large number in the GoM form through instabilities of shear layers. These instabilities interest both the edges of along-slope bottom-intensified boundary currents and the cores of these currents whenever confined over steep slopes (Bracco et al., 2016; Bracco et al., 2018). Near-bottom submesoscale circulations are particularly relevant for connectivity studies because they enhance diapycnal mixing through large vertical velocities at their edges, they can trap larvae in their cores and transport them along the bottom boundary layer, but also contribute to isolate them from the surrounding environment (Cardona and Bracco, 2016; Vic et al., 2018). There are no direct observations of submesoscale structures along the GoM continental slope; indirect confirmation was, however, provided by the mapping of the deep plume following the 2010 Deepwater Horizon blow-up (Camilli et al., 2010; Diercks et al., 2010). After validating the model representation of diapycnal dispersion along the continental shelf with the limited observations available in the GoM, we deployed neutrally buoyant virtual larvae at each site multiple times over the course of 2 years, 2015 and 2016. The model integrations aim

at investigating if physical processes play a role in structuring populations of *C. delta* in the Gulf of Mexico. The genetic data integrates over a much longer time period compared with the physical model that was forced by two years of data. The focus on a much shorter time horizon in the model run is due to the high horizontal and vertical model resolution required to adequately resolve the bathymetric details relevant to tracer advection and therefore larval dispersal. A high-resolution model is also necessary to capture the submesoscale dynamics that contribute to lateral and diapycnal mixing at scales relevant to the sites considered here (Bracco et al., 2016). Furthermore, a high-resolution, yet short-time scale model can be particularly informative if the results from the model are congruent with the genetic results.

Potential connectivity between sites was evaluated accounting for the possibility that larvae may diffuse vertically, enabling us to examine the depth differentiation hypothesis in greater detail. Results obtained with the biophysical model were then compared to the genetic analyses using both microsatellite and RAD-seq data concluding that physical isolation due to depth differences is the driving force shaping connectivity patterns in this species.

2. Material and Methods

For the purposes of this study, we focus our analyses on two pairs of sites where *C. delta* aggregations exist to the west of the Mississippi Fan in the northern Gulf of Mexico: MC751 (28.194N, -89.799W, 440 m) and MC885 (28.066N, 89.712W, 629 m), and GC235 (27.739N, 91.194W, 532 m) and GC249 (27.724N, 90.514W, 789 m). These sites are each relatively close in horizontal distance (15 km, and 69 km apart, respectively), but approximately 200 m apart in vertical distance (**Figure 1**). Another known population of *C. delta* occurs to the east of the Mississippi Fan (Etnoyer and Warrenchuk, 2007), but exhibits very limited connectivity with the four sites investigated here (Quattrini et al., 2015). The Fan indeed acts as an advection barrier as explored in detail in previous works (Bracco et al., 2016; Cardona et al., 2016).

Samples of *C. delta* were collected from these sites in 2009, 2010, and 2017 utilizing remotely operated vehicles (ROVs). In 2009 and 2010, colonies were sampled using the ROV Jason and the NOAA Ship Ron Brown. In 2017, the ROV Global Explorer and R/V Ocean Project were used. Branches were subsampled from each colony using coral cutters mounted on the ROV

manipulator arm; to minimize damage, the majority of colonies were left intact. Onboard each vessel, tissue samples were preserved in-duplicate in 95% cold (-20 deg C) EtOH and flash frozen in either liquid nitrogen or at -80 deg C. Further sampling details can be found in Quattrini et al. (2015).

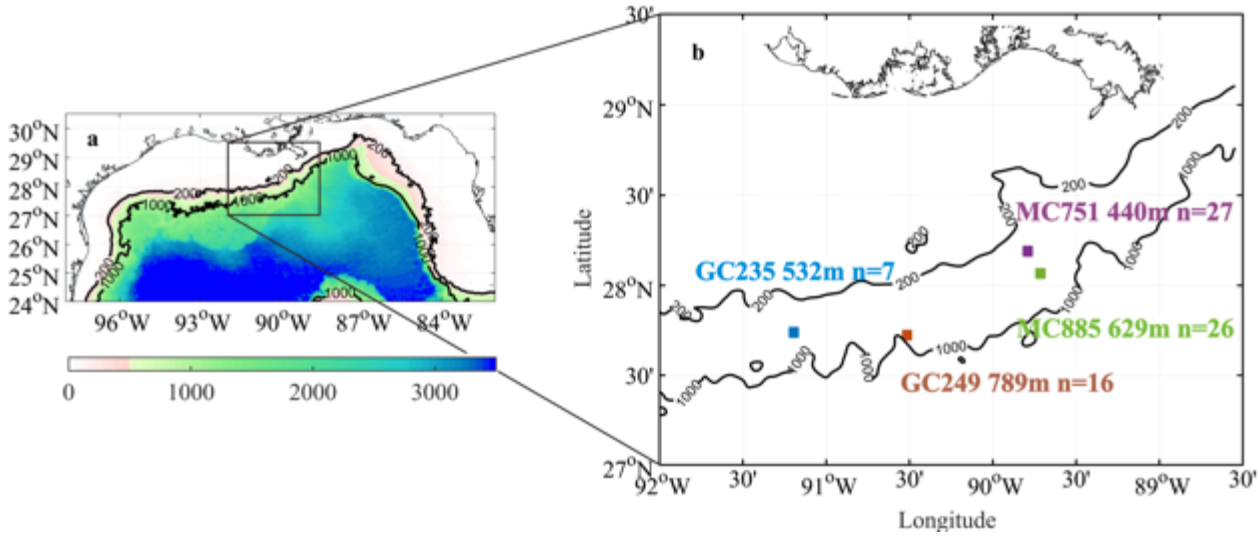

Figure 1. (a) Model domain and bathymetry with (b) zoom on the area of the *C. delta* sampling sites: MC751 (purple), MC885 (green), GC235 (blue), and GC234 (red).

2.1. Model set-up

We used the Coastal and Regional Ocean Community model (CROCO, https://www.croco-ocean.org/) to model the GoM ocean circulation. CROCO is a new, public modeling system built upon ROMS (Regional Ocean Modeling System) and is designed for simulating high-resolution offshore and nearshore dynamics in regional domain configurations (Shchepetkin and McWilliams 2005; Debreu et al. 2012). CROCO is a split-explicit, free-surface, and terrain-following vertical coordinate oceanic model that we configured over the GoM with a horizontal resolution of 1 km and 50 vertical layers. Rotated mixing tensors in lieu of horizontal diffusion and the K-Profile Parameterization (KPP) vertical mixing scheme (Large et al., 1994) are applied as mixing parameterizations for sub-grid processes. Horizontal tracer advection is discretized with split and rotated 3rd-order upstream-biased advection scheme. The model bathymetry is derived from the 1 min Gridded Global Relief Data (ETOPO1) topography (Amante and Eakins, 2008) interpolated to the model grid and modified to reduce horizontal pressure gradient errors using

201 the Sikiric et al. (2009) method, with maximum slope factor (r_0) of 0.25 and maximum hydrostatic
202 inconsistency number (r_1) of 15. The model domain extends over the northern GoM covering the
203 basin north of 24° N (**Figure 1**). It has open boundaries to the east and south sides that were
204 nudged to the 6-hourly Hybrid Coordinate Ocean Model - Navy Coupled Ocean Data Assimilation
205 (HYCOM-NCODA) Analysis system (GOMI0.04/expt_31.0,
206 http://www7320.nrlssc.navy.mil/hycomGOM). HYCOM-NCODA data are also used as initial
207 conditions. Six-hourly wind stresses and heat fluxes as well as daily precipitation from the
208 European Centre for Medium-Range Weather Forecast ERA-interim reanalysis (Dee et al., 2011)
209 were used to force CROCO. Daily fresh water discharge from United State Geological Survey
210 (USGS, http://waterdata.usgs.gov/nwis/rt) for the five major rivers (Mississippi, Atchafalaya,
211 Colorado, Brazos and Apalachicola) was applied. The corresponding volume flux was converted
212 to an equivalent surface salinity flux with a decay length scale of 35 km. Tides were not included,
213 given that the GoM has some of the lowest amplitude tides in the world. The tidal amplitude at the
214 coral colonies has been estimated to be less than 0.05 m (Gouillon et al., 2010).
215 After a spin-up to achieve equilibration, the model was run from October 15th 2014 to December
216 31th 2016. Instantaneous velocity and tracer fields (salinity, temperature) were saved every 5
217 days. Additionally, for each period during which connectivity was explored, hourly averages of the
218 three-dimensional velocity field were saved and used to advect over 3,000 virtual larvae off-line.
219 Because the pelagic larval duration (PLD) of *C. delta* is unknown, larvae were followed over 10,
220 20, and 40 days based on estimated PLD data for other deep-sea coral species (Brooke and
221 Järnegren, 2013; Graham et al., 2013; Cardona et al., 2016). The spawning time of *C. delta* is
222 also unknown; thus, larvae were released four times a year, one in each season, to explore the
223 possibility of a seasonal dependence. Hourly averaged velocity fields were saved from the 1st of
224 February May, August, and November to the 20th of the following month in both 2015 and 2016
225 and larvae were releases on the 1st, 6th, and 11th of each month.
226 This configuration is comparable to those used by Cardona et al. (2016) as far as resolution and
227 representation of near bottom distribution of vertical layers, and Barkan et al. (2017) for the
228 treatment of riverine inflow and surface fields. A verification of surface circulation, stratification
229 and currents was presented in these works. In particular, we verified that the range of observed

range of lateral speed at the depths of interest is reproduced by our model using Acoustic Doppler Current Profiler data (see Cardona et al., 2016). It should be noted, however, that the surface circulation is better constrained by abundant observations that the deep circulation, and is therefore more reliably modeled. The main difference between this and previous configurations reside in the domain size and the inclusion of open boundary conditions at 24^{o}N that allow for constraining the Loop Current and Loop Eddies positions (described further below) closer to observations.

A brief discussion on the modeled diapycnal mixing along the continental slope in the CROCO run can be found in the Appendix (Figure A.1).

The connectivity among *C. delta* sampling localities has been evaluated using the model output by advecting off-line about 4,500 (4489) neutrally buoyant Lagrangian particles in each season in 2015 and 2016. The virtual larvae are infinitesimally small and neutrally buoyant, while deepwater coral larvae have a finite size and may be slightly negatively buoyant (Miller, 1998; Brugler et al., 2013). The actual size is, however, very small compared to the model grid cell (1 km^2), so that the infinitesimally small approximation holds well, and buoyancy up to 10% heavier/lighter than the surrounding fluid does not influence in a significant way the transport whenever in presence of a flow field characterized by intense submesoscale circulations (Zhong et al., 2012). By doing so we neglect settling rates due to buoyancy that in idealized two-dimensional models without a realistic advection have been shown play an important role (Condie and Bormans, 1997).

The Lagrangian tracers are released near the ocean bottom in a 0.05^{o} x 0.05^{o} area centered at GC235, GC249, MC751 and MC885 (**Figure 1**) and are advected off-line by interpolating on the particle positions the modeled hourly-averaged three-dimensional velocities using LTRANS v.2b (Schlag and North, 2012). At 1 km horizontal resolution the resolved submesoscale circulations have life span longer than a day, and the use of hourly averaged fields introduces only a small error in the Lagrangian statistics (Keating et al., 2011), as previously verified (Choi et al., 2017). The parameterization of lateral mixing of momentum and tracers adopted in CROCO includes horizontal diffusion through a harmonic viscous term.

If the *C. delta* larvae are negatively buoyant to remain close to the ocean bottom, they may not diffuse effectively within the water column. However, due to the uncertainty associated with larval

buoyancy for this species, we also considered the possibility that larvae may diffuse in the vertical, adding a ‘‘vertical random walk” (Hunter et al., 1993) with an effective additional diffusion coefficient of 10^{-3} m^2s^{-1}. Furthermore, we assumed the size of the “arrival” area to be within a 0.1° x 0.1° domain around the observed colonies within +/- 30 m of the receiving site along the vertical. The arrival area is much larger than the colonies, and its size accounts in part for the interannual variability in the currents that is underestimated by considering only 2 years. Connectivity maps for an arrival area of 0.05° x 0.05° are available in the Appendix. We will show in the following results only relative to cases that include the vertical random walk. Finally, we explored how the connectivity potential may depend on the competency time and larval mortality. Following Wood et al. (2014), loss of competency is mathematically described by an exponentially decaying function:

$$P^{t+1} = P^t e^{-\lambda t} \quad \text{(eq. 1)},$$

where P^{t+1} quantifies how many larvae can settle at time t + 1 and λ is the decay constant linked to the pelagic larval duration (λ = ln(2)/(PLD/2)). The PLD was varied 10, 20 and 40 days. Particle tracking was terminated after 40 days.

All potential connectivity estimates are provided after testing all seasons in both years three times, with releases of modelled larvae 5 days apart.

2.4. Genetic data

Microsatellite Analyses

Microsatellite (e.g., tandem repeats in DNA sequences) data were obtained for 75 individuals of *C. delta* as described in Quattrini et al. (2015). Briefly, nine microsatellite loci were amplified with polymerase chain reaction across all individuals and subsequently analyzed on an ABI3130XL Genetic Analyzer (Univ. of Pennsylvania). A Bayesian model-based clustering approach, Structure (Pritchard et al., 2000), was used to determine the number of populations (designated by K) by assigning the probability of membership of individuals iteratively to each K. Model priors included LOCPRIOR, admixture, and correlated allele frequencies (Pritchard et al. 2000, Falush et al. 2003, Hubisz et al. 2009). Five independent chains of 1,000,000 MCMC generations were run following a burnin of 250,000 generations. Results from each of the five iterations were

aligned using CLUMPP v1.1(Jakobsson and Rosenberg, 2007) and plotted in DISTRUCT v 1.1 (Rosenberg 2004). To examine the amount of genetic differentiation among sampling localities, FST (Weir and Cockerham 1984) was calculated between sites and/or species (GENALEx). An Analysis of Molecular Variance (AMOVA) (Excoffier et al. 1992) was conducted to test for significance among pairwise FST (fixation index) values (GENALE v. 6.5, Peakall and Smouse, 2006).

Further methodological details can be found in Quattrini et al. (2015). Results from Structure and FST analyses were adapted from Quattrini et al. (2015).

RADSeq Analyses

Restriction site Associated DNA sequence (RAD-seq) data was obtained for 31 *C. delta* individuals (MC751 n=7; GC234 n=8; MC885 n=9; GC249 n=7) utilizing the 6-cutter restriction enzyme PstI, following the protocols described in Baird et al. 2008. We predicted between 32,000 and 110,000 cleavage sites for PstI in the *C. delta* genome using the program PredRAD (Herrera et al., 2015a). DNA was purified following protocols described in Herrera et al. (2015b). Concentration-normalized DNA (30ng/ul, 30ul volume) was submitted to Floragenex Inc (Eugene, OR) for library preparation and RAD sequencing. Libraries were multiplexed and sequenced using 10-base pair barcodes on an Illumina Hi-Seq 4000 platform (100 bp). This strategy yielded 5.9 ± 4.0 million raw sequence reads (average ± standard deviation) per individual. Reads were de-multiplexed and quality-filtered with the *process_radtags* program from the package Stacks v2.1 (Catchen et al., 2013) using the following flags: --inline_null, -r, -c, and -q, with default values. The Stacks *denovo_map* program was utilized to identify alleles at Single Nucleotide Polymorphisms (SNPs) and locus genotypes from each individual's filtered reads using the parameters -M 3 and -n 3.

The program *populations* (Catchen et al., 2013) was then used to select loci that were present in at least 50% of individuals within a sample site and in at least 3 of the 4 sites. This data matrix was exported as a structure file format, keeping only the first SNP per RAD locus. SNP data were summarized through a Principal components analysis (PCA) using the package adegenet v 2.1.1

in R v 3.5.1 (R Development Core Team, 2011), and F-statistics were calculated using custom scripts implementing the formulas by Weir & Cockerham (1984). The program *populations* was also used to produce a data matrix of haplotypes per RAD locus (multiple SNPs per locus), selecting loci that were present in at least 50% of individuals within a sample site and in all of the sites. These haplotype data were utilized to calculate an index of common ancestry (coancestry) among all individuals utilizing the program *fineRADstructure* (Malinsky et al. 2018).

4. Results

4.1 Modeled Circulation

Near the bottom and over the continental slope around the locations of the coral colonies, the time-averaged ocean circulation consists of intermittent, highly-variable along-shelf currents that follows bathymetric features, with a less pronounced seasonal cycle than at the surface. **Figure 2** shows near-bottom (about 15 m above bottom), daily-averaged currents, while the standard deviation of the zonal component *u*, based on daily-averaged data, is provided in the Appendix (Figure A.2). Winter emerges as the season with the strongest currents and variability, and summer with the least in both years considered.

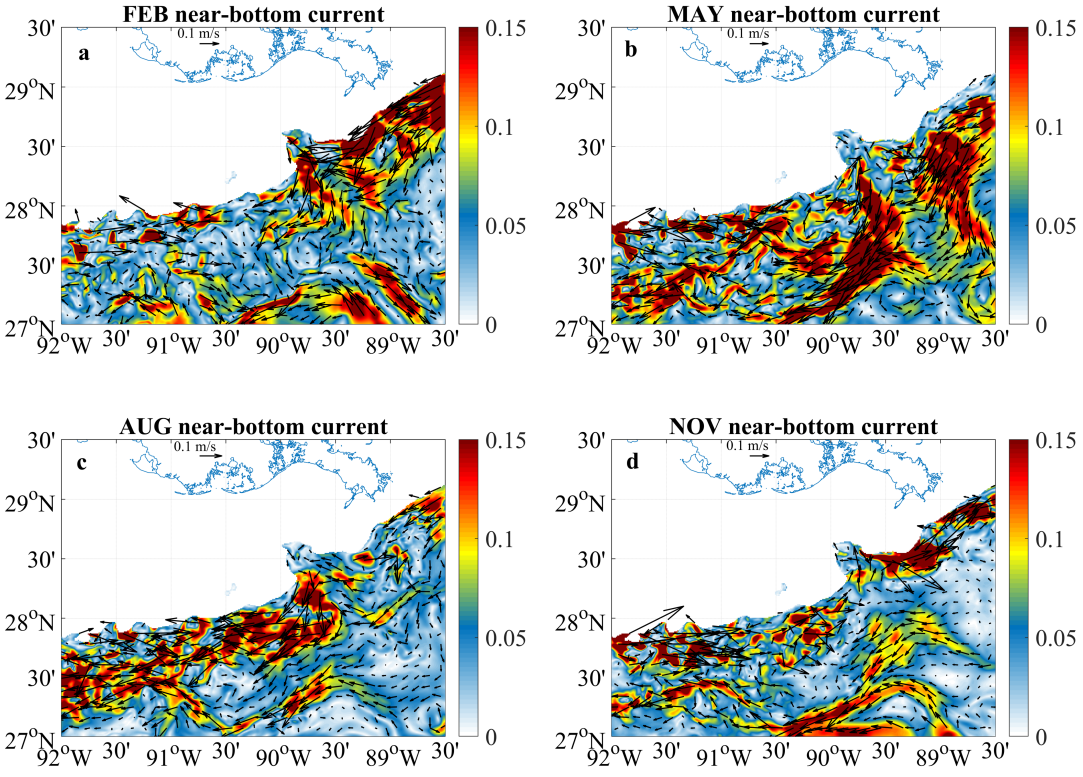

Figure 2. Daily averaged current speed (color) and lateral flow velocity (arrows) in the modeled bottom layers on the 10th of each month indicated on the panels in 2015 over the region of interest.

The complexity and variability of the current system over the continental slope is responsible for the generation of highly spatiotemporally-variable submesoscale circulations through instabilities of shear layers, that can be visualized in the vorticity field (**Figure 3**). Here vorticity is defined as $\frac{\varsigma}{f} = \frac{1}{f}\left(\frac{\partial v}{\partial x} - \frac{\partial u}{\partial y}\right)$, where ζ is relative vorticity, *f* the Coriolis parameter and *u* and *v* zonal and meridional velocity components. These submesoscale features, in the forms of small eddies and vorticity filaments, have trapping properties and are responsible for a non-zero lateral divergence field that controls the mixing.

Some surface mesoscale eddies also contribute to the transport at depth, extending to the top several hundred meters and encroaching into the shelf. An example of surface vorticity distribution is provided in Appendix (Figure A.3).

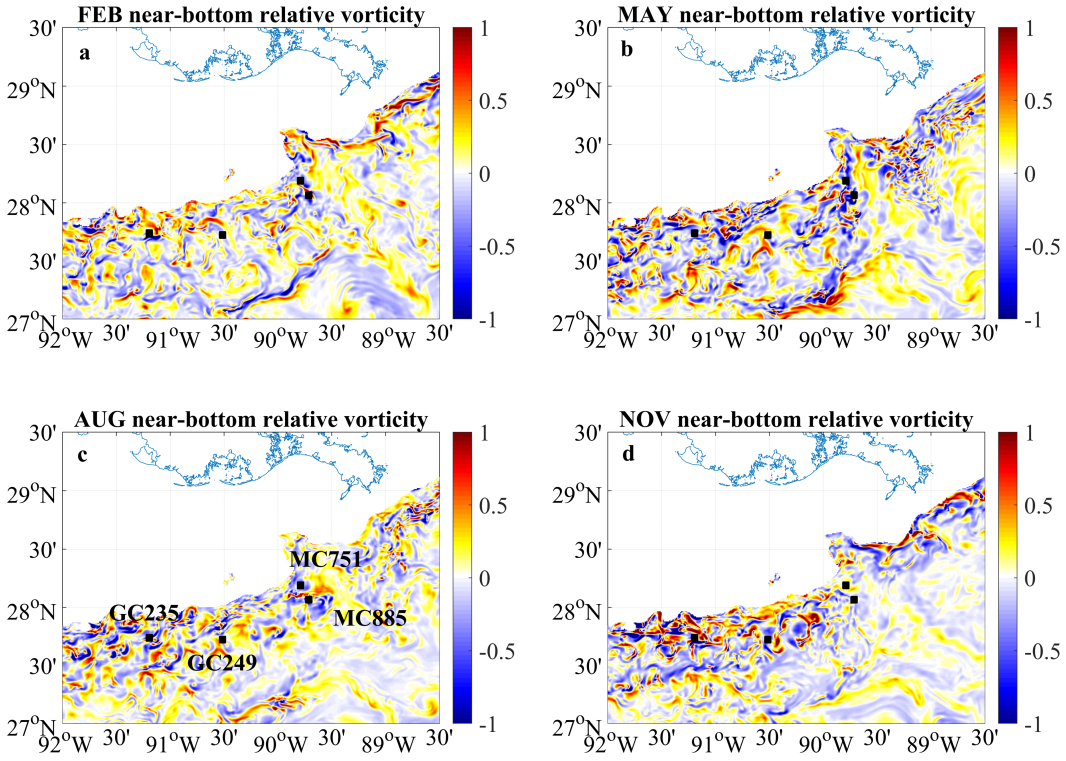

Figure 3. Instantaneous snapshots of relative vorticity normalized by the Coriolis parameter (ζ/f) in the modeled bottom layer on the 10th of each month indicated on panels in 2015 over the region where the *C. delta* colonies (black dots) are located.

352

353 **4.2. Modeled connectivity**

354 The particles released near the ocean bottom at the four sites moved prevalently, but not
355 exclusively, to the east in all seasons and both years. The modeled connectivity figures focused
356 on February and August, but potential connectivity was investigated also for May and November
357 and is provided in the table that summarizes this work.

358 In **Figure 4** the Lagrangian particles were not subject to mortality and were advected for 30 days.
359 In the left panels they were advected by the flow without any additional vertical diffusion, and they
360 followed well delineated filaments and vorticity structures that evolved within the density layer at
361 their formation site. In the right panels, on the other hand, they also underwent a vertical random
362 walk and their lateral diffusion increased, given that the greater vertical spreading enhanced the
363 particle's ability to escape the submesoscale structures that trapped them. In all cases, particles
364 advected at the edge of mesoscale eddies underwent the largest diapycnal excursions.

365

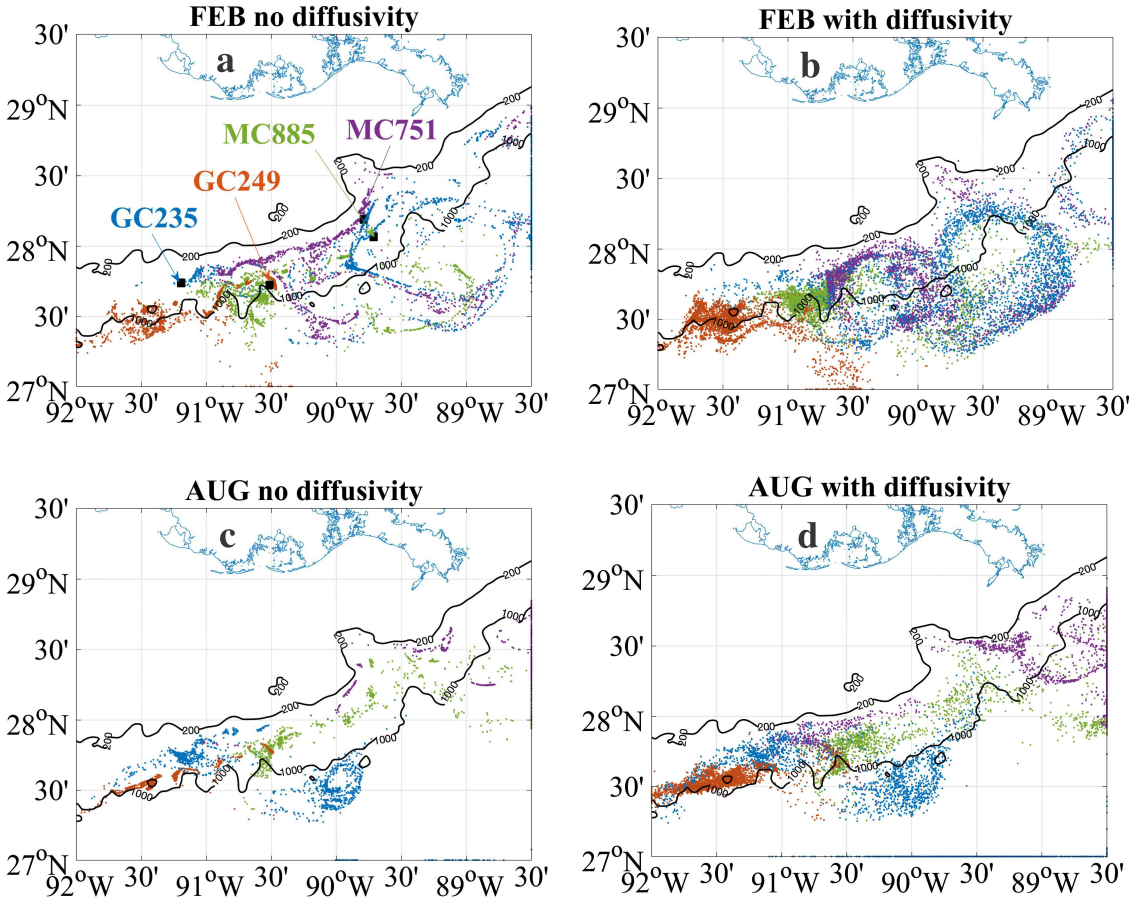

366

367 **Figure 4.** Lateral dispersion of Lagrangian particles released at the four sites in February (a-b)
368 and August (c-d) 2015, without (a-c) and with (b-d) additional vertical diffusivity in the form of a
369 random walk. The color of the particles corresponds to their release site, indicated in panel (a).
370
371 It is clear from these figures that lateral connectivity is high between the four sites, and virtual
372 larvae can easily spread on the horizontal plane reaching most, if not all, others sites.
373 Connectivity, however, remained very limited, even in the extreme case of no mortality over 30
374 days, between GC235/GC249 and MC751/MC885 whenever the depth at which particles are
375 located was accounted. Indeed, GC235/GC249 and MC751/MC885 were laterally but not
376 vertically connected (**Figure 5**, shown for February only; August results are presented in the
377 Appendix, Figure A.4).

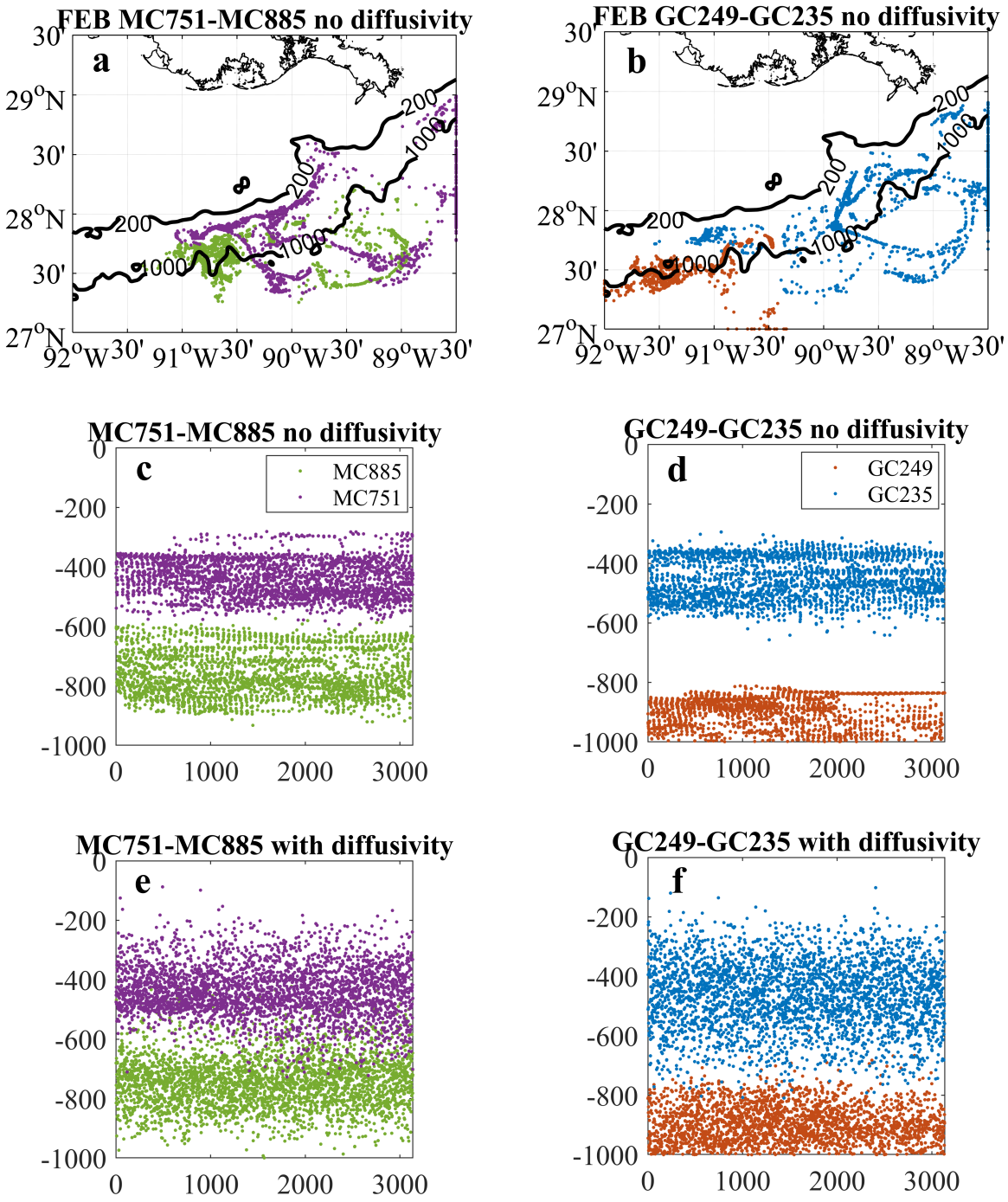

Figure 5. Lateral dispersion (a-b) and vertical dispersion without (c-d) and with additional diffusivity (e-f) for Lagrangian particles released at the MC sites (left column) and GC sites (right column) February 1st, 2015.

Potential connectivity results are summarized in **Figure 6**, where lateral only, and 3-dimensional (i.e. accounting for the vertical dimension) connectivity is provided for winter and summer, whenever the vertical random walk is included. We remind the reader that in the model, potential connectivity was considered achieved if particles 'arrived' within +/- 30 m of the receiving site

along the vertical and within a lateral box centered on the site of size 0.1° x 0.1° (Figure A.5 in the Appendix shows the corresponding connectivity maps for a receiving area of size 0.05° x 0.05°). Figure 6 summarizes the case (no mortality and additional vertical diffusion) with the highest potential connectivity of all those considered. The connectivity and its error in each estimate are calculated as the mean and standard deviation across three releases of virtual larvae from the four sites 5 days apart in each year (for example, across releases on August 1, 6 and 11, in 2015 and 2016).

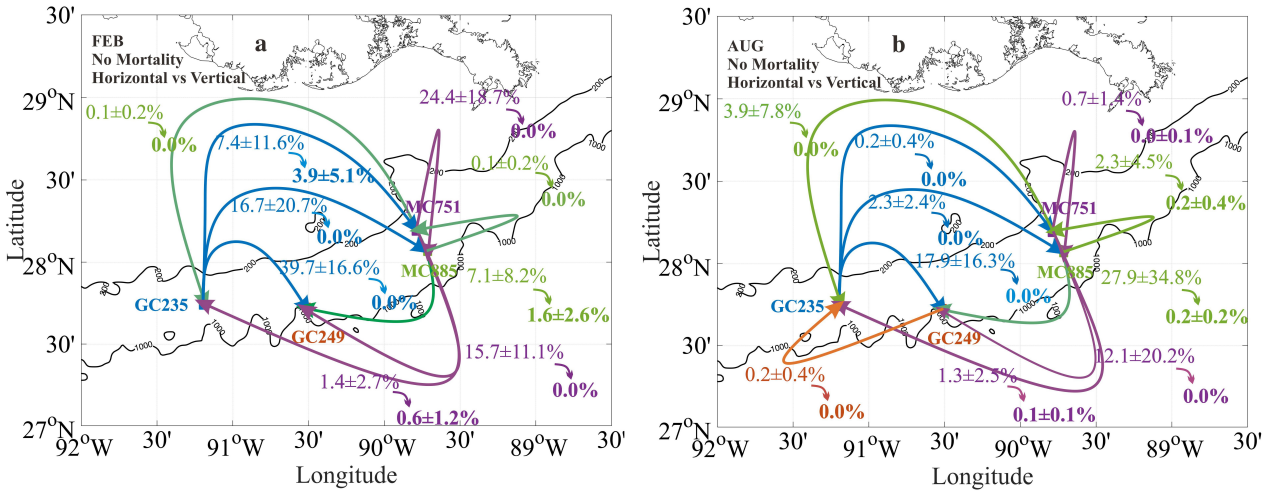

Figure 6 Horizontal only (light font) and three-dimensional (**bold** fonts) modeled connectivity potential in (a) February and (b) August calculated as mean +/- standard deviation over six releases of particles at the four sites. The releases are on day 1, 6 and 11 in each month in 2015 and 2016 and the Lagrangian tracers are followed for 30 days in the absence of a mortality term and with the addition of a vertical random walk. The color of the links indicates the site where the particles originated.

Potential connectivity tables for all seasons and releases, and for PLD = 20 and 40 days are provided in the Appendix (Tables A.1-A.3); in all cases values in the absence of an additional random walk connectivity values are different from zero only between GC235 and MC751.

4.2. Genetic analyses

Genetic differentiation of *C. delta* was evident among the four study sites in the study area. The Structure analysis of microsatellite data indicated that populations at GC249 and GC235 and

MC751 and MC885 were clearly differentiated from each other (**Figure 7a**). These results were independently supported by the analyses of RAD-seq data. The analysis of principal components showed clear differences in the genetic makeup between the sampling localities (**Figure 7b**), and both the principal components and the fineRADstructure indicated that individuals share a greater coancestry with other individuals from the same site than with individuals from other sites (**Figure 7c**). Pairwise FST values among populations (**Table 1**) indicate that the genetic differentiation is significant, and strongly suggest that depth is a determinant factor structuring the genetic diversity of *C. delta* populations in the northern GoM. A neighbor-joining dendrogram constructed with pairwise FST values calculated from SNP data indicate that shallower populations MC751 (440m) and GC235 (532m) are genetically more similar to each other than to either one of the deeper populations MC885 (629m) and GC249 (789m), in agreement with the modeled potential connectivity results (**Figure 7d**). Similarly, plots of pairwise FST data vs. depth differences among population sites show that there is a significant positive correlation between genetic differentiation and depth (Mantel Test p-value = 0.04, based on 999 replicates) (**Figure 7e**), but not with horizontal distance (**Figure 7f**).

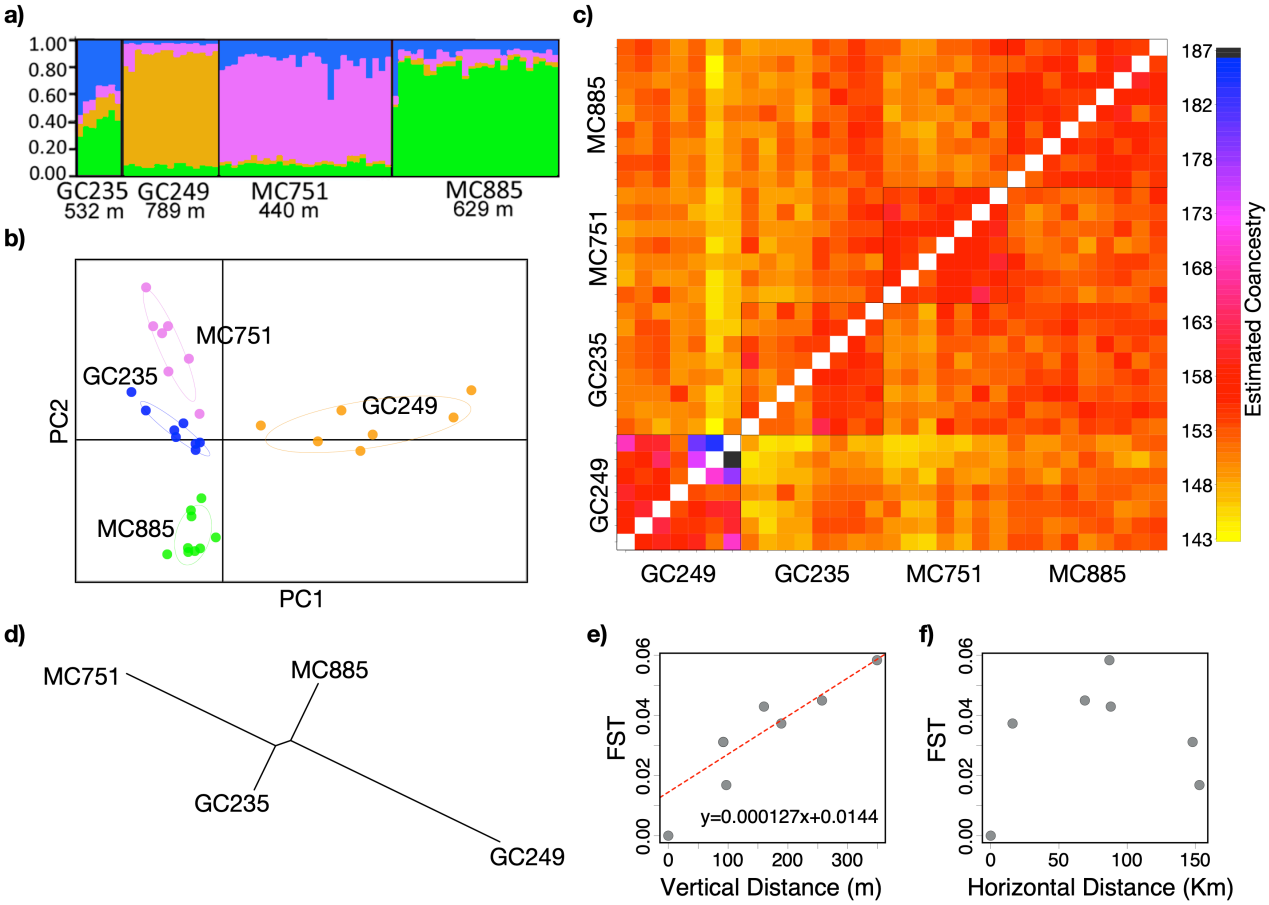

Figure 7. a) Average probability of membership for each individual coral (vertical bars) across the four target sites based on microsatellite data. b) Principal components analysis of *Callogorgia delta* genetic data using 61,179 SNP loci; each symbol represents an individual coral and colors indicate the sampling site. c) Clustered coancestry matrix generated with fineRADstructure using haplotype data; colors indicate pairwise coancestry estimates among all individuals. d) Neighbor-Joining dendrogram constructed with pairwise FST values (from SNPs) among populations e) Plot of depth differences vs. FST (from SNPs) for each pair of populations. Red line indicates best linear regression fit. f) Plot of horizontal distances vs. FST (from SNPs) for each pair of populations.

Table 1. Pairwise FST values between the four sites. P-values are included in parentheses for FST calculated using microsatellite data (adapted from Quattrini et al. 2015). 95% confidence intervals, calculated after 1000 bootstrap replicates, are included in parentheses for FST calculated from SNP data.

Pairwise FST microsatellites	**GC235**	**MC885**	**GC249**
MC751	0.036 (p=0.06)	0.032 (p=0.009)	0.047 (p=0.004)
GC234		0.039 (p=0.034)	0.038 (p=0.06)
MC885			0.028 (p=0.02)
Pairwise FST SNPs	**GC235**	**MC885**	**GC249**
MC751	0.031 (0.0267, 0.0356)	0.037 (0.032, 0.042)	0.058 (0.053, 0.064)
GC235		0.017 (0.013, 0.021)	0.045 (0.040, 0.050)
MC885			0.043 (0.038, 0.048)

5. Discussion

In the model, particles released at all four sites were transported along the isobaths in narrow currents following the bathymetric contours until they encountered mesoscale and submesoscale eddies that contributed to their off-shore advection. The role of coherent structures, especially eddies, was key for the advection around the MC sites, due to the formation of a large cyclone atop of the Mississippi Fan (see Bracco et al., 2016 for its formation mechanism) that extended into the water column to about 800 m. Shallower eddies, formed in all seasons through interactions with the bathymetry due to the presence of a canyon to the immediate east of the coral colonies (Bracco and Pedlosky, 2003), also influenced the lateral connectivity. As a result of the mesoscale activity around the canyon at depths of 300-500 m, particles released at the locations of the shallower colonies (GC235 and MC751) had larger horizontal dispersion than the other two.

Model potential connectivity was significantly different from zero only between GC235 and MC751 (in both directions, but preferentially from GC to MC) and, with smaller values, between MC885 and GC249. Very small connectivity was also found between MC885 and MC751. Their geographical proximity limited their potential connectivity given their substantial depth difference, even in presence of additional vertical diffusion to that exerted by the flow. We note that CROCO, despite the high resolution adopted, still slightly overestimates diapycnal mixing (see Suppl. Mat.); the real ocean is therefore likely to be less diffusive in the vertical than the model one.

The means and standard deviations presented, and the connectivity values found in each release, indicate that the weekly, not just interannual, variability are very large with respect to the lateral connectivity. According to the analysis of the model results, such behavior depends on the role that submesoscale and mesoscale eddies play on lateral transport.

In terms of seasonal dependence, the stronger currents in winter compared to summer tend to increase the lateral connectivity potential in this season across most sites. Nonetheless, independently of release considered, the potential connectivity is different from zero only between sites at approximately the same depth, and greater between the shallow ones (from GC235 to MC751).

469 The major outcome of this modeling work, summarized in Figure 6, is therefore the strong
470 limitation that depth poses on exchanges of larvae between geographically nearby sites. This is
471 consistent in all cases considered. Independently of how large the lateral connectivity may be, the
472 3-dimensional connectivity is mostly null if the sites are separated in depth by more than 150 m.
473 The outcome of the genetic analysis is that the patterns of time-integrated realized connectivity
474 are consistent with the short-term patterns of potential connectivity predicted by the circulation
475 and larval dispersal models. The very limited connectivity between colonies separated in depth is
476 confirmed. Together, the genetic and modeling results suggest that in the northern GoM depth, at
477 scales of tens to few hundreds of meters, is a stronger isolating factor for coral populations than
478 distance, at scales of tens to hundreds of kilometers. In the GoM depth differences on scales of
479 tens to few hundreds of meters constitute a strong physical isolating factor, limiting connectivity
480 for deepwater coral populations far more than distance. This behavior was associated, in the
481 model, with the presence of numerous mesoscale and submesoscale circulations generated by
482 the highly variable along-shore currents passing over the complex bathymetry that effectively
483 contribute to the horizontal transport, but do so through coherent (over few days to at most two
484 weeks) structures that trap material at their interior, limiting the diapycnal dispersion to their
485 vertical extent. Vertical migration of virtual larvae over as much as 40 days was no more than 50
486 m from the bottom in the absence of an explicit vertical diffusion term acting on the larvae, or at
487 most 100 m if an additional vertical random walk was considered. While this mechanism cannot
488 be generalized to other locations a priori, as it is not yet known how widely occurring energetic
489 submesoscale structures may be along continental shelfs and slopes, it is likely an important
490 player in other regions of the world ocean, where isolation by depth has been verified by genetic
491 methods (see Taylor and Roteman, 2017).
492 Furthermore, in this work little attention was paid to larval behavior, given that not much is known
493 about *C. delta* larvae (Etnoyer and Warrenchuk, 2007). Larval behavior may influence trapping
494 and settlement (Condie and Condie, 2016) but these properties are unconstrained for most
495 deepwater species and were therefore neglected.
496 It is important to stress once more that here the two frameworks adopted, genetic analysis and
497 modeling, cover different temporal scales; the first integrates over many generations of larval

498 dispersal events and other evolutionary mechanisms, while the circulation model was run for two
499 years, 2015 and 2016. It is unlikely that morphodynamic changes in the bathymetry in the GoM
500 were sufficiently large over the past few thousands of years to modify substantially the mean
501 characteristics of the circulation at the depth of the sites (Hill et al., 2011). Nonetheless, the
502 entirety of the current variability on interannual to decadal and longer scales cannot captured by a
503 two-year long run. The large size of the 'arrival' area and the addition of a vertical random walk
504 were chosen to partially compensate for the under-sampled variability. For many years to come
505 the high resolution required to capture the submesoscale circulations that control mixing on
506 scales of days to weeks will continue to limit the time length of regional ocean model integrations.
507 It is also worth mentioning that a circulation model at 1 km horizontal resolution does not include
508 all processes responsible for transport and mixing along the continental slope. Results shown
509 here, in Bracco et al. (2016) and in Cardona et al. (2016), however, suggest that 1 km represents
510 a good compromise between accuracy, reliability and computational costs. This may not be the
511 case for shallower corals along the shelf, for which the role of non-hydrodynamically balanced
512 processed, including internal and gravity waves, may need to be considered (Lentz et al., 2016),
513 despite the higher computational cost.
514
515 **6. Conclusions**
516 Deepwater corals, such as those found in the northern Gulf of Mexico, are foundational species
517 of the deep benthos. With continued anthropogenic threats to the marine environment, gathering
518 information about their connectivity properties is critically needed to allow informed
519 decisions about the management and conservation of these vulnerable ecosystems. Their scale
520 of dispersal indeed determines how colonies may recover from any disturbance. Such scale,
521 however, cannot be easily quantified through direct observations, due to the challenges
522 associated with measuring the deep ocean environment.
523 Here, we used genetic approaches integrated with an hydrodynamical circulation model of larval
524 dispersal to enhance our understanding of population connectivity of the deepwater coral
525 *Callogorgia delta*. We focused on four sites, separated laterally by as little as 15 km, but at
526 different depths, ranging from 440 m to 789 m. Genetic approaches and model outcome both

support the notion that connectivity across populations is limited, but it is strongest between the two shallower ones, found at similar depth, despite the larger geographical distance.

The integrated framework proposed allows for improving understanding of the geographic and depth-dependent footprint of larval dispersal, particularly in the deep seas. It also provides information that can be easily translated into smarter management decisions which is especially important in areas susceptible to anthropogenic disturbances such as the Gulf of Mexico. Ongoing initiatives at the Federal and State levels are seeking to protect areas of deepwater coral communities in the Gulf of Mexico. The research presented here indicates that the design of these protected areas should incorporate a 3D perspective. Both genetic and model data suggest that deepwater protected areas at similar depths are expected to be more connected to each other, than to areas at different depths, even if they their horizontal separation is small. However, this result should not be generalized until more studies examining diverse species and depth distributions, and larger sample sizes are available. A multi-species, multi-depth approach would help elucidate the factors driving connectivity of coral populations in the region.

Acknowledgements

This paper is a result of research funded by the National Oceanic and Atmospheric Administration's RESTORE Science Program under award NA17NOS4510096 to Lehigh University (SH, MPG), Georgia Tech (AB, GL) and Harvey Mudd College (AMQ). Sampling of *C. delta* was supplemented with previous collections from the Lophelia II project led by TDI-Brooks International and funded by BOEM and NOAA-OER (BOEM contract no. M08PC20038). The ROMS numerical simulations were funded in part by a grant from the Gulf of Mexico Research Initiative (GoMRI) through the ECOGIG consortium (ROMS output data are publicly available through the Gulf of Mexico Research Initiative Information & Data Cooperative at https://data.gulfresearchinitiative.org under doi:10.7266/n7-c8y1-sg06. We thank two anonymous reviewers for their comments that greatly improved the manuscript.

This is ECOGIG contribution # 532).

References

1. Amante, C., Eakins, B. W., 2008. ETOPO1 1 Arc-Minute Global Relief Model: Procedures, Data Sources and Analysis, National Geophysical Data Center, NESDIS, NOAA, U.S. Department of Commerce, Boulder, CO.
2. Baillon, S., Hamel, J.F., Wareham, V.E., Mercier, A., 2012. Deep cold-water corals as nurseries for fish larvae. Front. Ecol. Environ. 10, 351–356. doi:10.1890/120022
3. Baird, N. A., Etter, P. D., Atwood, T. S., Currey, M. C., Shiver, A. L., Lewis, Z. A., et al. 2008. Rapid SNP discovery and genetic mapping using sequenced RAD markers. PLoS One 3, e3376.
4. Barkan, R., McWilliams, J.C., Shchepetkin, A.F., Molemaker, J., Renault, L., Bracco, A., Choi, J., 2017. Submesoscale dynamics in the northern Gulf of Mexico. Part I: Regional and seasonal characterization, and the role of river outflow. J. Phys. Ocean, 47, 2325-2346, https://doi.org/10.1175/JPO-D-17-0035.s1.
5. Bongaerts P., Riginos C., Brunner R., Englebert N., Smith S.R., Hoegh-Guidberg O., 2017. Deep reefs are not universal refuges: Reseeding potential varies among coral species. Sci. Adv. 3. doi: 10.1126/sciadv.1602373.
6. Bracco, A., Choi, J., Joshi, K., Luo, H., McWilliams, J.C., 2016. Submesoscale currents in the northern Gulf of Mexico: Deep phenomena and dispersion over the continental slope. Ocean Model. 101, 43–58. doi:10.1016/j.ocemod.2016.03.002
7. Bracco, A., Choi, J., Kurian, J., Chang, P., 2018. Vertical and horizontal resolution dependency in the model representation of tracer dispersion in the northern Gulf of Mexico. Ocean Modell., 122, 13-25. doi:10.1016/j.ocemod.2017.12.008
8. Bracco, A., Liu, G., Sun, D., 2019. Mesoscale-submesoscale interactions in the Gulf of Mexico: From oil dispersion to climate. Chaos, Solitons & Fractals, 119, 63-72. https://doi.org/10.1016/j.chaos.2018.12.012
9. Bracco, A., Pedlosky, J., 2003. Vortex Generation by Topography in Locally Unstable Baroclinic Flows. J. Physic. Ocean. 33, 207-219. https://doi.org/10.1175/15200485(2003)033<0207:VGBTIL>2.0.CO;2

583 10. Brooke, S., Järnegren, J., 2013. Reproductive periodicity of the scleractinian coral
584 *Lophelia pertusa* from the Trondheim Fjord, Norway. Mar. Biol. 160, 139-153. doi:
585 10.1007/s00227-012-2071-x
586 11. Brugler, M.R., Opresko, D.M., France, S.C., 2013. The evolutionary history of the order
587 Antipatharia (Cnidaria: Anthozoa: Hexacorallia) as inferred from mitochondrial and nuclear
588 DNA: implications for black coral taxonomy and systematics. Zool. J. Linn. Soc., 169,
589 312–361. doi: 10.1111/zoj.12060
590 12. Camilli, R., Reddy, C.M., Yoerger, D.R., Van Mooy, B.A.S., Jakuba, M.V., Kinsey, J.C.,
591 McIntyre, C.P., Sylva, S.P., Maloney, J.V., 2010. Tracking hydrocarbon plume transport
592 and biodegradation at Deepwater Horizon. Science 330, 201–204. doi:
593 10.1126/science.1195223
594 13. Cardona, Y., Bracco, A., 2016. Predictability of mesoscale circulation throughout the
595 water column in the Gulf of Mexico. Deep Sea Res. Part II, 129, 332-349,
596 http://dx.doi.org/10.1016/j.dsr2.2014.01.008
597 14. Cardona, Y., Ruiz-Ramos, D. V., Baums, I.B., Bracco, A., 2016. Potential Connectivity of
598 Coldwater Black Coral Communities in the Northern Gulf of Mexico. PLoS One 11,
599 e0156257. doi:10.1371/journal.pone.0156257
600 15. Catchen, J., Hohenlohe, P. A., Bassham, S., Amores, A., and Cresko, W. A., 2013.
601 Stacks: an analysis tool set for population genomics. Mol. Ecol. 22, 3124–3140.
602 doi:10.1111/Mec.12354.
603 16. Condie, S.A., Bormans, M., 1997. The influence of density stratification on particle
604 settling, dispersion and population growth. J. Theoretical Biol., 187, 65-75.
605 17. Condie, S., Condie, R., 2016. Retention of plankton within ocean eddies. Global Ecology
606 and Biogeography, 25, 1264-1277.
607 18. Cordes, E.E., McGinley, M.P., Podowski, E.L., Becker, E.L., Lessard-Pilon, S., Viada,
608 S.T., Fisher, C.R., 2008. Coral communities of the deep Gulf of Mexico. Deep. Sea Res.
609 Part I, 55, 777–787. doi:10.1016/j.dsr.2008.03.005

610 19. Costantini, F., Gori, A., Lopez-Gonzalez, P., Bramanti, L., Rossi, S., Gili, J.M., Abbiati, M.,
611 2016. Limited Genetic Connectivity between Gorgonian Morphotypes along a Depth
612 Gradient. Plos One, 11, e0160678. doi: 10.1371/journal.pone.0160678.
613 20. Debreu, L., Marchesiello, P., Penven, P, Cambon, G., 2012. Two-way nesting in split-
614 explicit ocean models: algorithms, implementation and validation. Ocean Modelling 49-50,
615 1-21. https://doi.org/10.1016/j.ocemod.2012.03.003
616 21. Dee D.P., Uppala, S.M., Simmons, A.J., Berrisford, P., Poli, P., Kobayashi, S., et al.,
617 2011.The ERA-interim reanalysis: configuration and performance of the data assimilation
618 system. Quart. J. R. Meteorol. Soc. 137, 553–597, https://doi.org/10.1002/qj.828.
619 22. DeHaan, C.J., Sturges, W., 2005. Deep Cyclonic Circulation in the Gulf of Mexico. J.
620 Phys. Oceanogr. 35, 1801–1812. doi:10.1175/JPO2790.1
621 23. Demopoulos, A.W.J., Bourque, J.R., Frometa, J., 2014. Biodiversity and community
622 composition of sediment macrofauna associated with deep-sea Lophelia pertusa habitats
623 in the Gulf of Mexico. Deep. Sea Res. Part I 93, 91–103. doi:10.1016/j.dsr.2014.07.014
624 24. Diercks, A.R., Highsmith, R.C., Asper, V.L., Joung, D., Zhou Z., Guo, L., Shiller, A.M.,
625 Joye, S.B., Teske, A.P., Lohrenz, S.E., 2010. Characterization of subsurface polycyclic
626 aromatic hydrocarbons at the Deepwater Horizon site. Geophys. Res. Lett. 37, L20602,
627 doi:10.1029/2010GL045046
628 25. Donohue, K.A., Watts, D.R., Hamilton, P., Leben, R., Kennelly, M., 2016. Loop Current
629 Eddy formation and baroclinic instability. Dyn. Atmos. Oceans, 76, 195-216.
630 26. Etnoyer P. and Warrenchuk J., 2007. A catshark nursery in a deep gorgonian field in the
631 Mississippi Canyon, Gulf of Mexico. Bull. Mar. Sci. E. 8(3), 553-559.
632 27. Excoffier, L., Smouse, P.E., Quattro, J.M., 1992. Analysis of molecular variance inferred
633 from metric distances among DNA haplotypes: application to human mitochondrial DNA
634 restriction data. Genetics 131, 479-491
635 28. Falush, D., Stephens, M., Pritchard, J.K., 2003. Inference of population structure using
636 multilocus genotype data: linked loci and correlated allele frequencies. Genetics 164,
637 1567-1587.

638 29. Gaines, S.D., White, C., Carr, M.H., Palumbi, S.R., 2010. Designing marine reserve
639 networks for both conservation and fisheries management. Proc. Natl. Acad. Sci. U. S. A.
640 107, 18286– 93. doi:10.1073/pnas.0906473107
641 30. Gouillon, F., Morey, S. L., Dukhovskoy, D.S., O'Brien, J.J., 2010. Forced tidal response in
642 the Gulf of Mexico. J. Geoph. Res. 115, C10050, doi:10.1029/2010JC006122
643 31. Graham, E.M., Baird, A.H., Connolly, S.R., Sewell, M.A., Willis, B.L., 2013. Rapid declines
644 in metabolism explain extended coral larval longevity. Coral Reefs, 32, 539–549. doi:
645 10.1007/s00338-012-0999-4
646 32. Hamilton, P., Berger, T. J., Johnson, W., 2002. On the structure and motions of cyclones
647 in the northern Gulf of Mexico. J. Geoph. Res. – Oceans, 107, 3208–3226. doi:
648 10.1029/1999JC000270
649 33. Henry, L.A., Roberts, J.M., 2007. Biodiversity and ecological composition of
650 macrobenthos on cold-water coral mounds and adjacent off-mound habitat in the bathyal
651 Porcupine Seabight, NE Atlantic. Deep. Sea Res. Part I 54, 654–672.
652 doi:10.1016/j.dsr.2007.01.005
653 34. Herrera, S., Shank, T.M., 2016. RAD sequencing enables unprecedented phylogenetic
654 resolution and objective species delimitation in recalcitrant divergent taxa. Mol.
655 Phylogenet. Evol. 100, 70–79. doi:10.1016/j.ympev.2016.03.010
656 35. Herrera, S., Reyes-Herrera, P. H., and Shank, T. M., 2015a. Predicting RAD-seq marker
657 numbers across the eukaryotic tree of life. Genome Biol. Evol. 7, 3207–3225.
658 doi:10.1093/gbe/evv210.
659 36. Herrera, S., Watanabe, H., and Shank, T. M., 2015b. Evolutionary and biogeographical
660 patterns of barnacles from deep-sea hydrothermal vents. Mol. Ecol. 24, 673–689.
661 doi:10.1111/mec.13054.
662 37. Hill, D.F., Griffiths, S.D., Peltier, W.R., Horton, B.P., Törnqvist, T.E., 2011. High-resolution
663 numerical modeling of tides in the western Atlantic, Gulf of Mexico, and Caribbean Sea
664 during the Holocene. J. Geoph. Res. 116, C10014, doi: 10.1029/2010JC006896

665 38. Hubisz, M.J., Falush, D., Stephens, M., Pritchard, J.K., 2009. Inferring weak population
666 structure with the assistance of sample group information. Mol. Ecol. Resour. 9, 1322-32.
667 doi:10.1111/j.1755-0998.2009.02591.x
668 39. Hunter, J.R., Craig, P.D., Phillips, H.E., 1993. On the use of random walk models with
669 spatially variable diffusivity. J. Comput. Phys. 106, 366–376
670 40. Jakobsson, M., Rosenberg, N.A., 2007. CLUMPP: a cluster matching and permutation
671 program for dealing with label switching and multimodality in analysis of population
672 structure. Bioinformatics 23, 1801-1806.
673 41. Jahnke, M., Jonsson, P.R., Moksnes, P.O., Loo, L.O., Jacobi, M.N. & Olsen, J.L., 2018.
674 Seascape genetics and biophysical connectivity modelling support conservation of the
675 seagrass Zostera marina in the Skagerrak-Kattegat region of the eastern North Sea. Evol.
676 Appl., 11, 645-661.
677 42. Johns, W., Townsend, T., Fratantoni, D., Wilson, W., 2002. On the Atlantic Inflow to the
678 Caribbean Sea. Deep Sea Res. Part I 49, 211–243. doi: 10.1016/s0967-0637(01)00041-3
679 43. Jombart, T., Ahmet, I., 2011. *adegenet 1.3-1*: new tools for the analysis of genome-wide
680 SNP data. Bioinformatics, 27, 3070–3071. https://doi.org/10.1093/bioinformatics/btr521
681 44. Keating, S.R., Smith, K.S., Kramer, P.R. 2011. Diagnosing lateral mixing in the upper
682 ocean with virtual tracers: Spatial and temporal resolution dependence. J. Physical
683 Ocean., 41, 1512-1534.
684 45. Kinlan, B.P., Gaines, S.D., Lester, S.E., 2005. Propagule dispersal and the scales of
685 marine community process. Divers. Distrib. 11, 139–148. doi:10.1111/j.1366-
686 9516.2005.00158.x
687 46. Krieger, K.J., Wing, B.L., 2002. Megafauna associations with deepwater corals (Primnoa
688 spp .) in the Gulf of Alaska. Hydrobiologia 471, 80–92
689 47. Lal M.M., Southgate P.C., Jerry D.R., Bosserelle C., Zenger K.R., 2017. Swept away:
690 ocean currents and seascape features influence genetic structure across the 18,000 Km
691 Indo-Pacific distribution of a marine invertebrate, the black-lip pearl oyster *Pinctada*
692 *margaritifera.* BMC Genomics 18:66. doi: 10.1186/s12864-016-3410-y.

693 48. Large, W.G., McWilliams, J.C., Doney, S.C., 1994. Oceanic vertical mixing: a review and
694 a model with a nonlocal boundary layer parameterization. Rev. Geophys. 32, 363–403.
695 doi:10.1029/94RG01872
696 49. Lentz, S.J., Churchill, J.H., Davis, K.A., Farrar, J.T., Pineda, J., Starczak, V., 2016. The
697 characteristics and dynamics of wave-driven flow across a platform coral reef in the Red
698 Sea. J. Geophys. Res. - Oceans 121, 1360-1376.
699 50. Liu, G., Bracco, A., Passow, U., 2018. The influence of mesoscale and submesoscale
700 circulation on sinking particles in the northern Gulf of Mexico. Elementa, 6, 36,
701 http://doi.org/10.1525/elementa.292
702 51. Malinsky, M., Trucchi, E., Lawson, D. J., and Falush, D., 2018. RADpainter and
703 fineRADstructure: Population Inference from RADseq Data. Mol. Biol. Evol. 35, 1284–
704 1290. doi:10.1093/molbev/msy023.
705 52. Miller, K.J., 1998. Short-distance dispersal of black coral larvae: inference from spatial
706 analysis of colony genotypes. Mar. Ecol. Prog. Ser. 163, 225–233.
707 53. Morrison, C. L., Ross, S. W., Nizinski, M. S., Brooke, S., Järnegren, J., Waller, R. G., et al.
708 2011. Genetic discontinuity among regional populations of Lophelia pertusa in the North
709 Atlantic Ocean. Conservation Genetics, 12(3), 713-729.
710 54. Ohlmann, J.C., Niiler, P.P., 2005. Circulation over the continental shelf in the northern
711 Gulf of Mexico. Prog. Ocean., 64, 45-81, doi: 10.1016/j.pocean.2005.02.001
712 55. Ohlmann, J. C., Niiler, P. P., Fox, C. A., Leben, R. R., 2001. Eddy energy and shelf
713 interactions in the Gulf of Mexico. J. Geoph. Res. – Oceans, 106, 2605–2620.
714 56. Peakall, R., Smouse, P.E., 2006. GenAlEx 6: genetic analysis in Excel. Population genetic
715 software for teaching and research. Mol. Ecol. Notes. 6, 288–295.
716 57. Pritchard, J.K., Stephens, M., Donnelly, P., 2000. Inference of Population Structure Using
717 Multilocus Genotype Data. Genetics 155, 945-959.
718 58. Quattrini, A.M., Baums, I.B., Shank, T.M., Morrison, C.L., Cordes, E.E., 2015. Testing the
719 depth-differentiation hypothesis in a deepwater octocoral. Proc. Biol. Sci. 282, 20150008.
720 doi:10.1098/rspb.2015.0008

59. R Development Core Team, 2011. *R: A Language and Environment for Statistical Computing.* Vienna, Austria R Foundation for Statistical Computing.
60. Rosenberg, N.A., 2004. distruct: a program for the graphical display of population structure. Mol. Ecol. Res. 4, 137-138. https://doi.org/10.1046/j.1471-8286.2003.00566.x
61. Ross, S.W., Quattrini, A.M., 2009. Deep-sea reef fish assemblage patterns on the Blake Plateau (Western North Atlantic Ocean). Mar. Ecol. 30, 74–92. doi:10.1111/j.1439-0485.2008.00260.x
62. Rowden, A.A., Schlacher, T.A., Williams, A., Clark, M.R., Stewart, R., Althaus, F., Bowden, D.A., Consalvey, M., Robinson, W., Dowdney, J., 2010. A test of the seamount oasis hypothesis: Seamounts support higher epibenthic megafaunal biomass than adjacent slopes. Mar. Ecol. 31, 95–106. doi:10.1111/j.1439-0485.2010.00369.x
63. Schlag Z.R., North E.W. Lagrangian TRANSport model (LTRANS v.2) User's Guide. University of Maryland Center for Environmental Science, Horn Point Laboratory. Cambridge, MD, 183. (2012) (available at: http://northweb.hpl.umces.edu/LTRANS/LTRANSv2/ LTRANSv2_UsersGuide_6Jan12.pdf).
64. Shchepetkin, A.F., McWilliams J.C., 2005. The regional oceanic modeling system (ROMS): a split-explicit, free-surface, topography-following-coordinate oceanic model. Ocean Modelling 9, 347–404. doi: 10.1016/j.ocemod.2004.08.002
65. Sikiric, M.D., Janeković, I., Kuzmić, M., 2009. A new approach to bathymetry smoothing in sigma-coordinate ocean models. Ocean Mod. 29, 128-136. doi: 10.1016/j.ocemod.2009.03.009
66. Sinclair, E.A., Ruiz-Montoya, L., Krauss, S.L., Anthony, J.M., Hovey, R.K., Lowe, R.J. & Kendrick, G.A., 2018. Seeds in motion: Genetic assignment and hydrodynamic models demonstrate concordant patterns of seagrass dispersal. Mol. Ecol., 27, 5019-5034.
67. Stone, R.P., 2006. Coral habitat in the Aleutian Islands of Alaska: depth distribution, fine-scale species associations, and fisheries interactions. Coral Reefs 25, 229-238, doi: 10.1007/s00338-006-0091-z

68. Taylor, M. L., Roterman, C. N., 2017. Invertebrate population genetics across Earth's largest habitat: The deep-sea floor. Molecular ecology, *26*(19), 4872-4896.
69. Vic, C., Gula, J., Roullet, G., Pradillon, F., 2018. Dispersion of deep-sea hydrothermal vent effluents and larvae by submesoscale and tidal currents. Deep Sea Res. Part I 133, 1-18, doi: 10.1016/j.dsr.2018.01.001
70. Waters, J.M., Condie, S.A. & Beheregaray, L.B., 2014. Does coastal topography constrain marine biogeography at an oceanographic interface? Mar. Freshwater Res., 65, 969-977
71. Weir, B.S., Cockerham, C.C., 1984. Estimating F-Statistics for the analysis of population-structure. Evolution 38, 1358–1370.
72. White, C., Selkoe, K.A., Watson, J., Siegel, D.A., Zacherl, D.C. & Toonen, R.J., 2010. Ocean currents help explain population genetic structure. Proc. R. Soc. B. 277, 1685-1694.
73. Wood, S., Paris, C.B., Ridgwell, A., Hendy, E.J., 2014. Modelling dispersal and connectivity of broadcast spawning corals at the global scale. Global Ecol. Biogeogr. 23, 1–11, https://doi.org/10.1111/geb.12101
74. Yesson, C., Wright, E., Braga-Henriques, A., 2018. Population genetics of Narella versluysi (Octocorallia: Alcyonacea, Primnoidae) in the Bay of Biscay (NE Atlantic). Mar. Biol., 165, 135. doi:10.1007/s00227-018-3394-z.
75. Zhong, Y., Bracco, A., 2013. Submesoscale impacts on horizontal and vertical transport in the Gulf of Mexico. J. Geoph. Res. - Oceans 118, 5651-5668, doi:10.1002/jgrc.20402
76. Zhong, Y., Bracco, A., Villareal, T. A., 2012. Pattern formation at the ocean surface: Sargassum distribution and the role of the eddy field. Limn. Ocean.: Fluids Envir. 2, 12–27, doi: 10.1215/21573689-1573372

Appendix

Diapycnal mixing evaluation

A key quantity required for a realistic representation of larval potential connectivity in light of the problem examined in this work is the diapycnal mixing rate around the coral sites. To our knowledge there are no direct observations of such rate in the region and depths of interest, where the model estimate is $k_z \sim 1 \times 10^{-3}$ m^2 s^{-1}. However, in August 2012 a passive dye was injected near the 2010 Deepwater Horizon spill site at approximately 1100 m and was followed over twelve months with a first cruise four months after release (Ledwell et al., 2016). This experiment allowed for constraining diapycnal mixing along the continental slope of the northern Gulf of Mexico in the deep layer (i.e. below 1000 m). Values observed four months after the release were comprised between $k_z \sim 1.3 \times 10^{-4}$ - 4×10^{-4} m^2 s^{-1}. Under the assumption that a model performing well in terms of mixing rates below 1000 m, is also reliable at shallower depths, we seeded the area east of 89°W with (De Soto Canyon, where the Deepwater Horizon was located) with passive Lagrangian particles at depths comprised between 1000 and 1500 m on February, May, August, and November 1st, 2015 and evaluated the diapycnal mixing over 40 days. Figure A.1 shows the resulting modelled diapycnal mixing, averaged across the four deployments (see Bracco et al., 2016 for more details on the calculation), which is close to the one-point in time observational estimates. Noting, however, that diffusivities tend to grow over time for releases in De Soto Canyon (see Fig. 15 in Bracco et al., 2016), we anticipate an overall stronger diapycnal diffusivity in the model compared to real ocean.

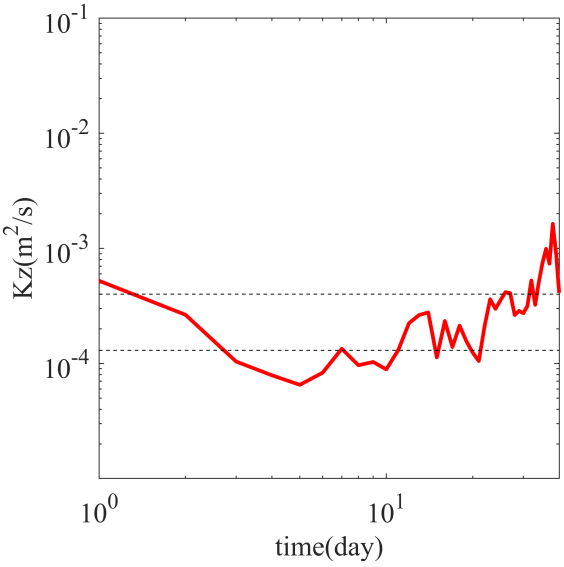

795

796 **Figure A.1** Diapycnal diffusivity over time (in red) calculated using Lagrangian tracer
797 deployments around the location of the deep release experiment (Ledwell et al., 2016). The two
798 values computed by Ledwell et al. (2016) from profiles from stations seaward and shoreward of
799 the 1500 m isobaths 4 months after a dye release are also indicated by the dashed black lines.

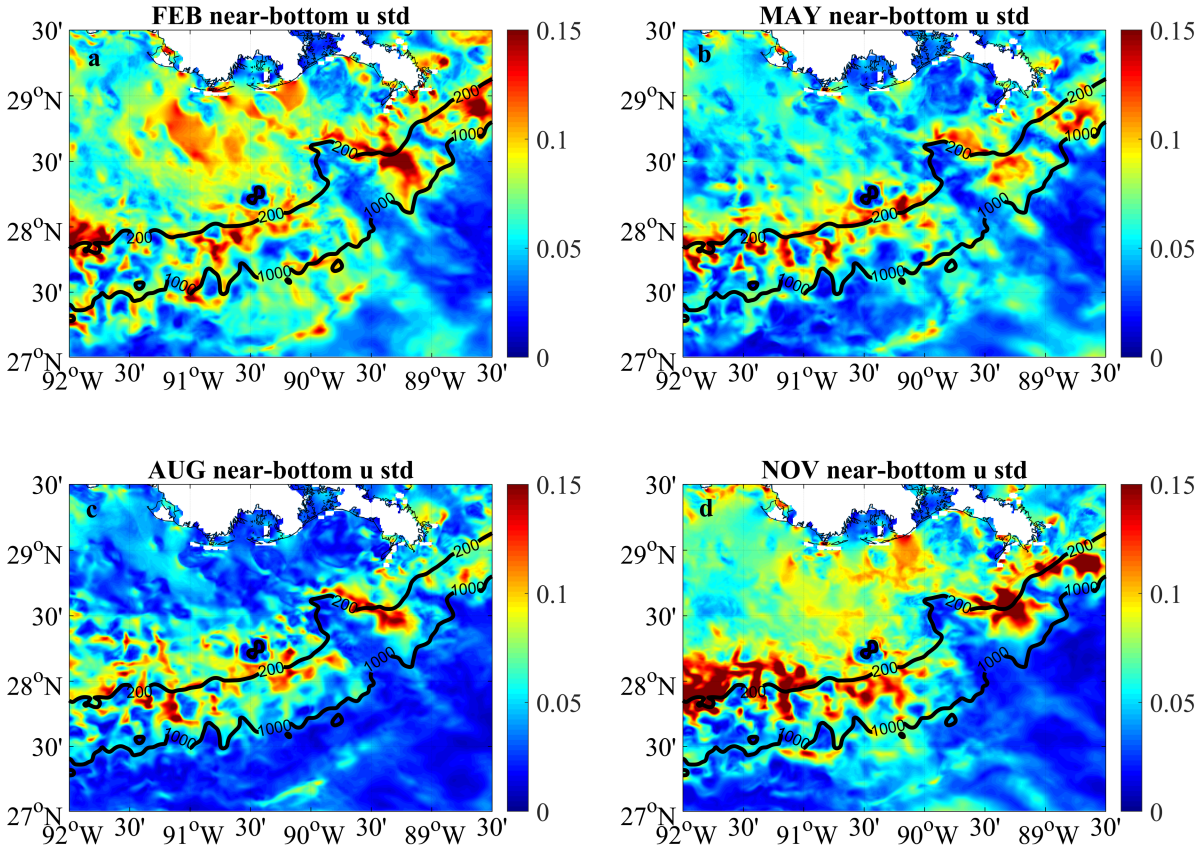

800

801

802 **Figure A.2** Standard deviation (STD) of the zonal component of the near-bottom velocity (u
803 component) in each of the seasons considered. The STD is calculated using hourly averaged
804 velocities taken every 6 hours over 40 days (for example, from August 1st to September 10th) and
805 over 2015 and 2016. The variability is strongest in winter (followed by fall) and weakest in summer.
806 The same seasonal cycle holds for near bottom relative vorticity, as highly variable currents are
807 subject to submesoscale instabilities. Differences between winter and summer are statistical
808 significant (P value < 0.05). Differences between winter and the other two seasons are significant
809 only at the 10% level.

810 Unit: m s^{-1}

811

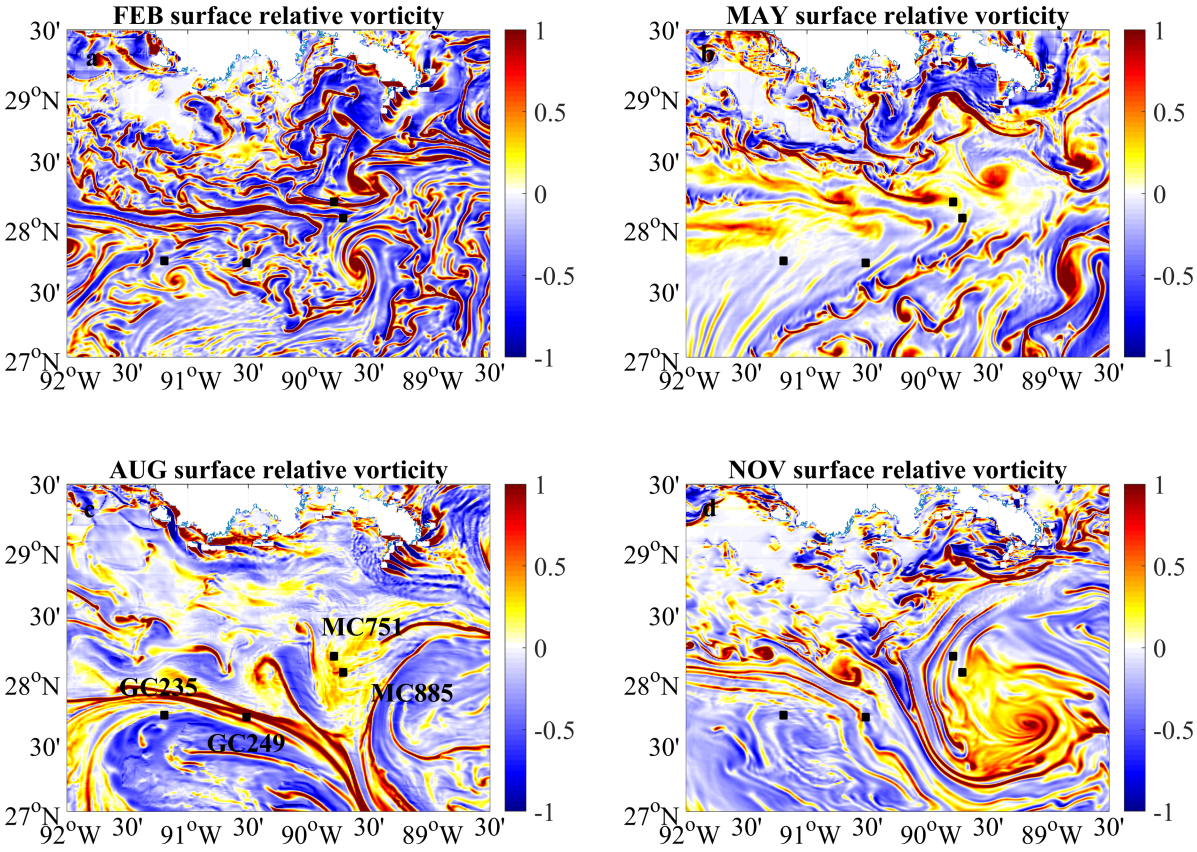

812

813 **Figure A.3** Instantaneous snapshots of relative vorticity normalized by the Coriolis parameter

814 (ζ/f) at the ocean surface on the 10th of each month indicated on panels in 2015 over the area

815 where the *C. delta* colonies (black dots) are located.

816

817

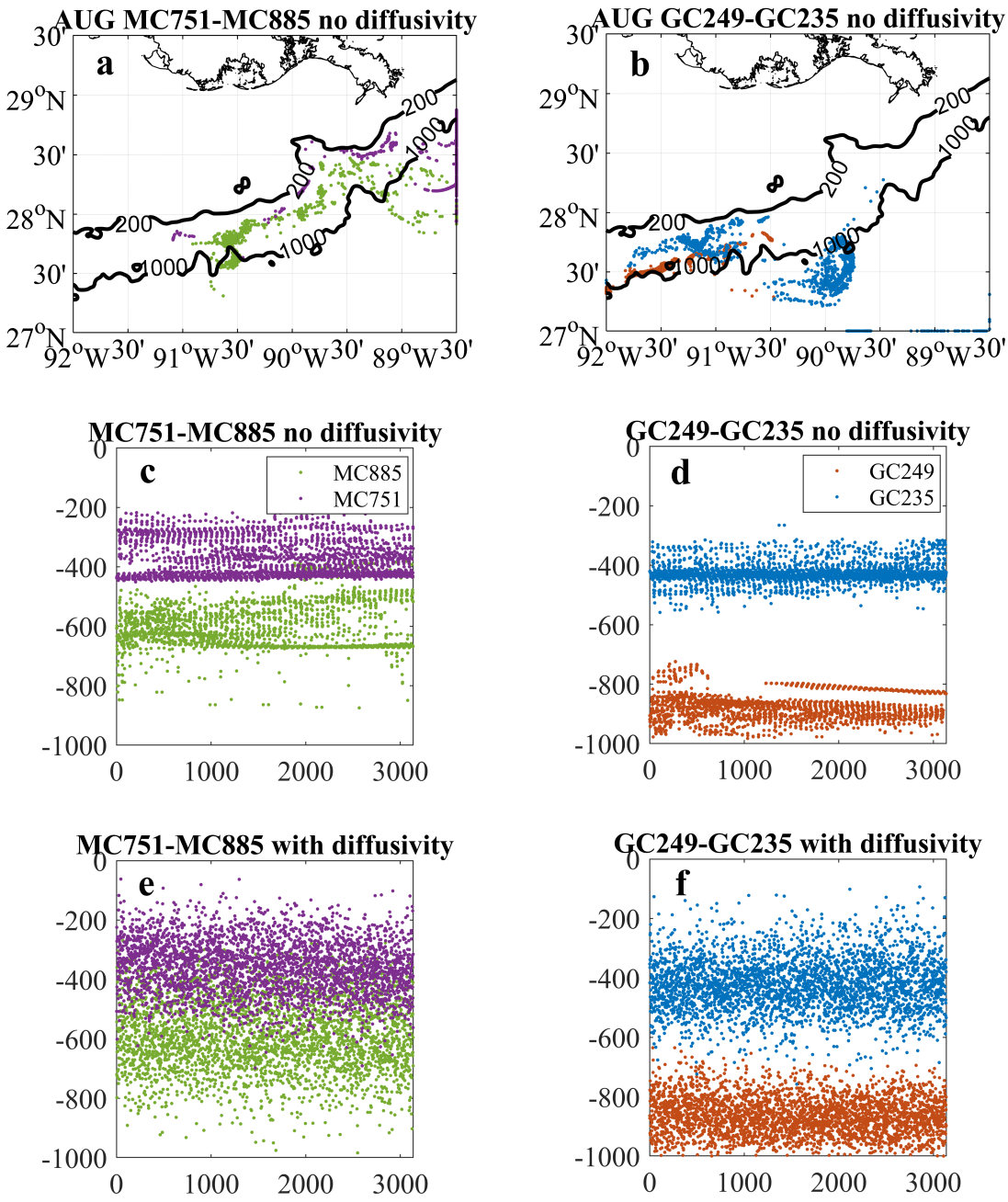

Figure A.4 Lateral dispersion (a-b) and vertical dispersion without (c-d) and with additional diffusivity (e-f) for Lagrangian particles released at the MC sites (left column) and GC sites (right column) August, 1st 2015.

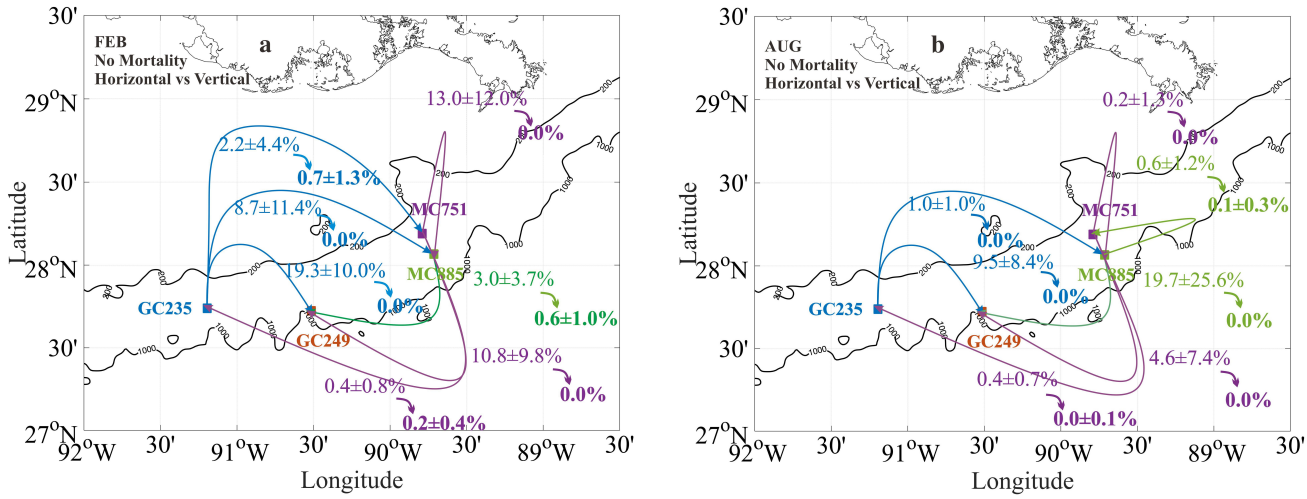

Figure A.5 Horizontal only (light font) and three-dimensional (**bold** fonts) modeled connectivity potential in (a) February and (b) August calculated as mean +/- standard deviation over six releases of particles at the four sites with an arrival area of 0.05° x 0.05° (instead of 0.1° x 0.1° in Figure 6). The releases are on day 1, 6 and 11 in each month in 2015 and 2016 and the Lagrangian tracers are followed for 30 days in the absence of a mortality term and with the addition of a vertical random walk. The color of the arrows indicates the site where the particles originated.

837 Connectivity potential: Summary Tables

	MC885	MC751	GC249	GC235
Feb-MC885	-	0.1±0.2% **0.0%**	7.1±8.2% 1**.6±2.6%**	0.1±0.2% **0.0%**
Feb-MC751	24.4±18.7% **0.0%**	-	15.7±11.1%. **0.0%**	1.4±2.7% **0.6±1.2%**
Feb-GC249	0.0% **0.0%**	0.0% **0.0%**	-	0.0% **0.0%**
Feb-GC235	16.7±20.7% **0.0%**	7.4±11.6% **3.9±5.1%**	39.7±16.6%. **0.0%**	-
May-MC885	-	0.1±0.1% **0.0%**	5.7±9.9% **0.5±0.8%**	0.2±0.3% **0.0%**
May-MC751	39.5±37.1% **0.0%**	-	5.8±8.4% **0.0%**	0.1±0.1% **0.0%**
May-GC249	0.0% **0.0%**	0.0% **0.0%**	-	0.2±0.4% **0.0%**
May-GC235	25.5±10.5% **0.0%**	12.7±4.2% **6.1±7.2%**	46.2±21.0%. **0.0%**	-
Aug-MC885	-	2.3±4.5% **0.2±0.4%**	27.9±34.8% **0.2±0.2%**	3.9±7.8% **0.0%**
Aug-MC751	0.7±1.4% **0.0±0.1%**	-	12.1±20.2%. **0.0%**	1.3±2.5% **0.1±0.1%**
Aug-GC249	0.0% **0.0%**	0.0% **0.0%**	-	0.2±0.4% **0.0%**
Aug-GC235	2.3±2.4% **0.2±0.4%**	0.2±0.4% **0.0%**	17.9±16.3%. **0.0%**	-
Nov-MC885	-	0.4±0.5% **0.1±0.2%**	12.7±21.9%. **0.0%**	0.0% **0.0%**
Nov-MC751	13.7±14.3% **0.0%**	-	12.7±11.0%. **0.0%**	0.0% **0.0%**
Nov-GC249	0.0% **0.0%**	0.0% **0.0%**	-	0.3±0.3% **0.0%**
Nov-GC235	7.0±5.8% **0.0%**	4.2±4.2% **2.5±2.4%**	34.2±28.2% **0.0%**	-

838

839 **Table A.1** Connectivity potential (mean and standard deviation) calculated over six releases in
840 February, May, August and November 2015 and 2016 in the absence of a mortality term and
841 calculated over 30 days in the presence of a vertical random walk. Lateral connectivity on top,
842 three-dimensional connectivity underneath in bold.

843

844

845

846

847

	MC885	MC751	GC249	GC235
Feb-MC885	-	0.0% **0.0%**	1.5±1.4% **0.3±0.5%**	0.0% **0.0%**
Feb-MC751	15.9±13.1% **0.0%**	-	3.6±2.8%. **0.0%**	0.3±0.6% **0.2±0.3%**
Feb-GC249	0.0% **0.0%**	0.0% **0.0%**	-	0.0% **0.0%**
Feb-GC235	4.9±6.6% **0.0%**	1.7±2.6% **0.9±1.2%**	22.5±14.8%. **0.0%**	-
May-MC885	-	0.0% **0.0%**	1.8±3.1% **0.1±0.2%**	0.0.% **0.0%**
May-MC751	30.0±32.6% **0.0%**	-	2.8±3.1% **0.0%**	0.0.% **0.0%**
May-GC249	0.0% **0.0%**	0.0% **0.0%**	-	0.0% **0.0%**
May-GC235	11.3±7.6% **0.0%**	2.7±0.4% **1.0±1.0%**	30.4±14.1%. **0.0%**	-
Aug-MC885	-	1.2±2.4% **0.1±0.1%**	10.3±14.0% **0.1±0.1%**	1.1±2.1% **0.0%**
Aug-MC751	0.4±0.3% **0.0%**	-	3.3±5.4%. **0.0%**	0.5±1.0% **0.0%**
Aug-GC249	0.0% **0.0%**	0.0% **0.0%**	-	0.0% **0.0%**
Aug-GC235	0.4±0.5% **0.0%**	0.0% **0.0%**	11.2±12.0%. **0.0%**	-
Nov-MC885	-	0.1±0.1% **0.0%**	6.9±11.9%. **0.0%**	0.0% **0.0%**
Nov-MC751	6.7±6.0% **0.0%**	-	7.4±6.5%. **0.0%**	0.0% **0.0%**
Nov-GC249	0.0% **0.0%**	0.0% **0.0%**	-	0.0% **0.0%**
Nov-GC235	1.6±1.4% **0.0%**	0.9±1.1% **0.5±0.6%**	25.3±24.92% **0.0%**	-

848 **Table A.2** Connectivity potential (mean and standard deviation) calculated over six releases in
849 February, May, August and November 2015 and 2016 in the case of PLD = 40 days in the presence
850 of a vertical random walk. Lateral connectivity on top, three-dimensional connectivity underneath
851 in bold.

852

853

854

	MC885	MC751	GC249	GC235
Feb-MC885	-	0.0% **0.0%**	3.1±3.5% **0.8±1.3%**	0.0% **0.0%**
Feb-MC751	19.6±15.4% **0.0%**	-	7.3±5.2%. **0.0%**	0.7±1.4% **0.3±0.7%**
Feb-GC249	0.0% **0.0%**	0.0% **0.0%**	-	0.0% **0.0%**
Feb-GC235	9.1±11.9% **0.0%**	3.6±5.6% **2.1±2.7%**	29.3±15.4%. **0.0%**	-
May-MC885	-	0.1±0.1% **0.0%**	3.1±5.3% **0.2±0.3%**	0.1±0.1% **0.0%**
May-MC751	33.9±34.8% **0.0%**	-	4.0±5.8% **0.0%**	0.0 % **0.0%**
May-GC249	0.0% **0.0%**	0.0% **0.0%**	-	0.1±0.1% **0.0%**
May-GC235	16.2±8.5% **0.0%**	5.4±1.0% **2.6±3.1%**	37.5±17.6%. **0.0%**	-
Aug-MC885	-	1.5±3.1% **0.2±0.4%**	16.6±22.3% **0.1±0.1%**	2.1±4.2% **0.0%**
Aug-MC751	0.9±0.9% **0.0%**	-	6.3±10.4%. **0.0%**	0.7±1.4% **0.0%**
Aug-GC249	0.0% **0.0%**	0.0% **0.0%**	-	0.1±0.2% **0.0%**
Aug-GC235	1.1±1.2% **0.0%**	0.1±0.2% **0.0%**	13.9±13.9%. **0.0%**	-
Nov-MC885	-	0.2±0.3% **0.1±0.2%**	9.3±16.1%. **0.0%**	0.0% **0.0%**
Nov-MC751	9.3±0.2% **0.0%**	-	9.7±8.4%. **0.0%**	0.0% **0.0%**
Nov-GC249	0.0% **0.0%**	0.0% **0.0%**	-	0.1±0.1% **0.0%**
Nov-GC235	3.1±2.7% **0.0%**	1.9±2.0% **1.1±1.0%**	28.9±26.4% **0.0%**	-

855 **Table A.3** Connectivity potential (mean and standard deviation) calculated over six releases in
856 February, May, August and November 2015 and 2016 in the case of PLD = 20 days in the presence
857 of a vertical random walk. Lateral connectivity on top, three-dimensional connectivity underneath
858 in bold.

859

860

861

862